Nanoscale

RSC Publishing

PAPER

View Article Online
View Journal | View Issue

Cite this: *Nanoscale*, 2013, **5**, 4388

Double-sided ZnO nanorod arrays on single-crystal Ag holed microdisks with enhanced photocataltytic efficiency†

Yuanhui Zuo,‡[a] Yao Qin,‡[b] Chao Jin,[a] Ying Li,[a] Donglu Shi,[b] Qingsheng Wu*[ac] and Jinhu Yang*[ab]

Received 14th December 2012
Accepted 11th February 2013

DOI: 10.1039/c3nr34102j

www.rsc.org/nanoscale

Novel hierarchical heterostructures of double-sided ZnO nanorod (NR) arrays grown on single-crystal Ag holed microdisks (HMDs) have been prepared through a two-step aqueous strategy including ZnO seed loading and the subsequent heteroepitaxial growth of ZnO NRs on Ag HMDs. By simply adjusting the synthetic parameters, ZnO NRs with variable NR diameters (20–200 nm), lengths (100–1.8 μm) and unusual shapes (concave, tubular and sharp tips) on Ag HMDs have been realized, which endows the Ag/ZnO heterostructures with versatile morphologies. The novel Ag/ZnO heterostructures consisting of integrated 1D semiconductor/2D metal nanostructured blocks with high specific surface area (SSA) and opened spatial architectures may promise important applications related to photoelectric fields. As expected, in photocatalytic measurements, the typical Ag HMD/ZnO NR heterostructure exhibits superior catalytic activity over other catalysts of bare ZnO NRs, ZnO NR arrays or heterostructured Ag nanowires (NWs)/ZnO NRs. The synergistic effect of the unique Ag HMD/ZnO NR heterostructures contributing to the high catalytic performance has been discussed in detail.

1 Introduction

Recently, nanoheterostructures of materials have become a hot research field and attracted increasing interest due to their potential to endow materials with novel functions and enhanced performances.[1–10] Among these, semiconductor–metal heterostructures have emerged as an important class because of their unique optical, electrical, catalytic and magnetic properties[3–7,11,12] and promising wide applications. It is well known that as a typical noble metal, Ag shows high electrical conductivity and good resistance to corrosion.[13–16] On the other hand, ZnO is an important wide-bandgap (3.37ev) semiconductor with abundant easy-to-prepare morphologies and optical, electrical and catalytic properties.[17–22] Therefore, the incorporation of ZnO and Ag into integrated heterogeneous nanostructures has received special attention.[4,11,23–28] Owing to their superior physical/chemical properties, Ag–ZnO heterostructures have shown great potential in a variety of fields, including photocatalysis,[23–26] solar-energy conversion,[27] microelectronics,[28] as well as surface-enhanced Raman scattering (SERS) applications.[29]

It is generally recognized that effective charge separation and transfer at the interfaces of semiconductor and metal components are the fundamental working principles to achieve enhanced performance in applications, which is a basic criterion for the rational design and fabrication of semiconductor–metal heterostructures.[24,30] It is reported that a variety of Ag–ZnO nanostructures with different structures and dimensions have been prepared including Ag nanoparticles (NPs)/ZnO NPs,[25,26] Ag NPs/ZnO nanorods (NRs)[4,11,23] or Ag NPs/ZnO hollow sphere arrays,[29] and ZnO NRs/Ag nanowires (NWs).[24] However, these heterostructures are often realized by simply depositing or modifying Ag NPs on ZnO NPs or NRs and mainly consist of isolated phases of the two components.[4,11,23,25,26,29] This will certainly create abundant crystal interfaces with many defects and electron traps, which are disadvantageous to the transport and output of carriers and overall performance of these heterostructure-based devices. Focusing on this problem, we have recently fabricated delicate fluffy-like heteroassemblies consisting of one dimensional (1D) ZnO NRs and Ag NWs, namely, ZnO branched NR arrays grown on Ag core NWs.[30] This novel heterostructure assembled by 1D nanostructure units is capable of delivering direct and fast electron transport through ZnO NRs or Ag NWs and thereby achieving high performance in related utilizations, for example, the high-efficiency photocatalysis of Rhodamine B (RhB) photodegradation.[30]

[a]*Department of Chemistry, Tongji University, Siping Road 1239, Shanghai 200092, People's Republic of China. E-mail: yangjinhu2010@gmail.com; qswu@tongji.edu.cn*

[b]*Institute for Biomedical Engineering & Nano Science, Tongji University, Siping Road 1239, Shanghai 200092, People's Republic of China*

[c]*Key Laboratory of Yangtze River Water Environment, Ministry of Education, Shanghai 200092, PR China*

† Electronic supplementary information (ESI) available: Synthesis of ZnO seeds (S1), dispersed ZnO NRs (S2) and ordered ZnO NR arrays on ITO substrates (S3) and SEM images of ZnO NR arrays (Fig. S1). See DOI: 10.1039/c3nr34102j

‡ These authors contributed equally to this work.

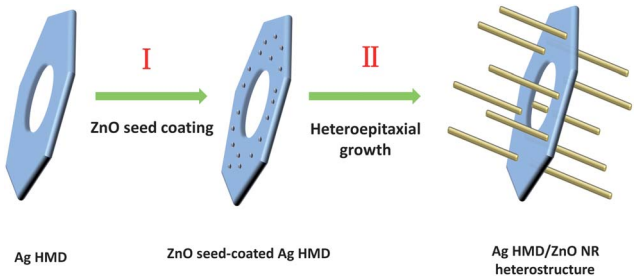

Scheme 1 A schematic illustration of the procedure for the controllable synthesis of the hierarchical Ag HMD/ZnO NR heterostructures *via* the aqueous solution approach.

However, compared with that of two dimensional (2D) structures, the 1D electron transport of Ag NWs is still not efficient enough, from the viewpoint of spatial configuration. In this context, we therefore extend the synthetic strategy to a more advanced hierarchical Ag/ZnO heterostructure where ZnO NR arrays are grown on both sides of the 2D single-crystal Ag holed microdisks (HMDs) realized through a two-step process involving ZnO seed coating and subsequent heteroepitaxial growth of ZnO NRs (see Scheme 1). Moreover, it was found that the diameter, length and shape of the ZnO NRs and the morphology of the heterostructure are finely tunable. The novel Ag HMD/ZnO NR heterostructure shows unique structural advantages: (i) high specific surface area (SSA). The double-sided ZnO NR arrays offer a double SSA and more active sites compared to conventional single-sided ones. (ii) Highly efficient charge separation and transport. The structure of the double-sided ZnO NR arrays on Ag microdisks provides integrated contact of the two components, which is conducive to efficient separation of photoinduced changes at their interfaces. Meanwhile, ZnO NRs and Ag HMDs serve as 1D and 2D pathways for fast electron transport, which in turn also benefits charge separation. (iii) Diffusion kinetics facilitation. The double-sided ZnO NR arrays on the holed Ag microdisks have a special spatial configuration, which allows high rate molecular diffusion for free access and exit through the structure. Therefore, with these merits, the novel hierarchical Ag/ZnO heterostructure may have important potential in a variety of fields related to solar cells, lithium batteries, sensors and photocatalysis as well. To the best of our knowledge, this is first time that the novel hierarchical heterostructures of Ag HMDs/ZnO NRs have been prepared. In addition, the as-prepared Ag/ZnO heterostructure displays remarkable photocatalytic activity in RhB degradation compared with other bare ZnO NR counterparts, which is attributed to the synergistic effect of its unique structure.

2 Experimental section

2.1 Materials

The anionic dextran (Dex-40, M_w 40 000) and dextran sulfate (DexS-40, M_w 40 000) were purchased from Roth (Germany). All of the other chemical reagents were of analytical grade, and the water used was deionized.

2.2 Preparation of Ag HMDs

Ag HMDs were prepared by our previously reported method[31] with modification. Briefly, 0.1 g of DexS-40 was added into a mixed solution containing 5 mL of formamide and 4.8 mL of water under vigorous stirring. Then, 0.1 mL of 0.2 M ascorbic acid was added when the DexS-40 was completely dissolved. Finally, 0.1 mL of 0.2 M $AgNO_3$ was added in the mixed solution with stirring, giving a turbid solution with a final reactant concentration of 2 mM. The solution was aged at room temperature for 24 h, resulting in a grey precipitate. The product was collected with the centrifuge method, redispersed by sonication, washed by water three times, dried in air and kept for further use.

2.3 Preparation of the ZnO NR arrays on Ag HMDs

For the typical synthesis, the Ag HMDs were firstly soaked in 0.1 g L^{-1} poly-(vinylpyrrolidone) (PVP) aqueous solution for ~4 h, followed by washing with ethanol to remove excessive adsorbed PVP molecules. Then, the PVP-treated Ag HMDs were dispersed in the prepared ZnO seed solution (S1†). After 4 h, the Ag HMDs with coated ZnO seeds were separated and washed with ethanol twice. Subsequently, the obtained ZnO seed-coated Ag HMDs were cast onto a clean ITO substrate (2 cm × 2 cm). After full evaporation of ethanol, the ITO substrate covered with uniform ZnO seed-coated Ag HMDs was dried for 1 h to ensure a strong adhesion of Ag HMDs to the substrate. Then, the substrate was suspended upside down in a 20 mL aqueous solution composed of equimolar zinc nitrate (0.01 M) and hexamethylenetetramine (HMT) (0.01 M). After incubation at 85 °C for 8 h, the substrate was removed from the solution, rinsed thoroughly with deionized water, and dried in air.

2.4 Characterization

The morphology was characterized using a scanning electron microscope (SEM, Hitachi S4800, 3 kV) and high-resolution transmission electron microscopy (HR-TEM, JEM 2011, 200 kV). The crystal structure was determined by X-ray diffraction (XRD) using a D/max2550VB3+/PC X-ray diffractometer with Cu Kα radiation with a 1.5418 Å wavelength. A beam voltage of 40 kV and a 100 mA current beam were used. The UV-vis spectra of the samples were recorded on a Cary-50 UV-vis spectrophotometer.

2.5 Photocatalysis evaluation

The ITO substrate (2 cm × 2 cm) covered with the Ag HMD/ZnO NR heterostructures obtained under typical conditions was immersed in 10 mL of 5 mg L^{-1} rhodamine B (RhB) aqueous solution. After 1 h stirring in the dark with full adsorption of RhB on the catalysts, the system was irradiated by a 300 W high-pressure mercury lamp. The samples were taken out from solution at a given time interval and measured by a UV-vis spectrometer (Varian Cary 500) to determine the residual RhB in solution.

3 Results and discussion

Fig. 1 shows the typical heterostructures of the ZnO NR arrays on Ag HMDs. From an overview SEM image in Fig. 1A, it can be observed that the products were formed at a large scale on the substrate, giving a forest-like morphology. The Ag/ZnO heterostructures whose sizes were about 4–6 μm can be distinguished by their outlines, as labeled with circles in different colors. However, it is difficult to find Ag HMDs in the heterostructures due to the dense covering of ZnO NR arrays on their surfaces. The XRD pattern of the Ag/ZnO heterostructures (Fig. 1B) displays clearly two sets of diffraction peaks corresponding to the fcc-structured silver and the hexagonal-structured wurtzite ZnO (JCPDS, no. 36-1451), respectively, which confirms that the heterostructures were composed of Ag and ZnO. In Fig. 1C, an individual Ag HMDs/ZnO NRs heterostructure circled in yellow is selected for close observation, which exhibits a symmetric shape with a Ag HMD (indicated by the red dashed line) as the symmetry plane covered by ZnO NR arrays on both its sides. Generally, these ZnO NRs are ~80 nm in diameter and 1–1.2 μm in length, judging from the close view of a magnified SEM image in Fig. 1D. Furthermore, the corresponding TEM characterizations (Fig. 1E and F) demonstrate that the ZnO NRs are single crystals with good crystallinity and take a growth direction of [0002] that is typical for ZnO NRs.[30,32,33]

Ag HMDs employed for constructing the above hierarchical Ag/ZnO heterostructures (Fig. 1) were prepared *via* a developed dextran-directed growth approach in a formamide–water mixed solution, where dextran with SO_4^{2-} group modification served as an effective additive to promote the Ag microdisk formation.[31] Fig. 2A presents a typical SEM image of the Ag HMDs. It can be seen that the Ag microdisks show a good dispersity with an average diameter of ~4 μm, and interestingly, almost every Ag microdisk had one or several holes with sizes ranging from ~50 nm to ~2 μm. Fig. 2B shows a magnified image where the Ag HMDs exhibit a roughly hexagonal shape and a disk thickness of ~50 nm (Fig. 2B, inset), giving an average aspect ratio of ~80. The formation of holes is likely to be due to the dissolution of unstable defects initially formed in the Ag disks at a high nucleation and growth rate, leaving holes in the central position of the disks. A similar phenomenon has been found in the aqueous-solution growth of ZnO nanodisks.[34] The structural characteristics are confirmed by the corresponding TEM image (Fig. 2C). In addition, the electronic diffraction (ED) pattern taken from an individual Ag HMD displays a set of clear spots with hexagonal symmetry which are readily assigned to metallic silver with face-centered cubic (fcc) structure (JCPDS, no. 04-783) (Fig. 2D). This result suggests that the Ag HMD is a single crystal with its top face bound by the {111} planes.[31] The XRD pattern in Fig. 2E shows sharp reflections corresponding to the fcc structure of silver with the (111) reflection intensified considerably, confirming that the HMDs are made of pure silver and their top face plane is the (111) plane. As ZnO seeds were proven to be crucial for ZnO NR growth on different substrates,[30] they were precoated onto Ag HMDs with the

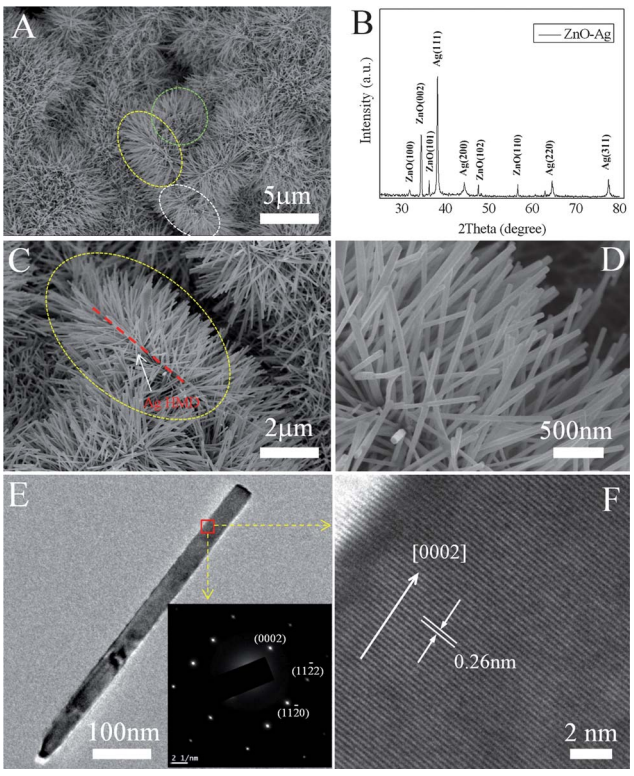

Fig. 1 SEM (A, C and D), TEM (E) and high-resolution TEM (F) images and XRD pattern (B) of Ag HMD/ZnO NR heterostructures formed under typical conditions. Growth time: 8 h; zinc nitrate concentration: 10 mM. The insets of (E) and (F) are the ED pattern and crystal lattice analysis, respectively, corresponding to the squared area (in red) of the ZnO NR in (E).

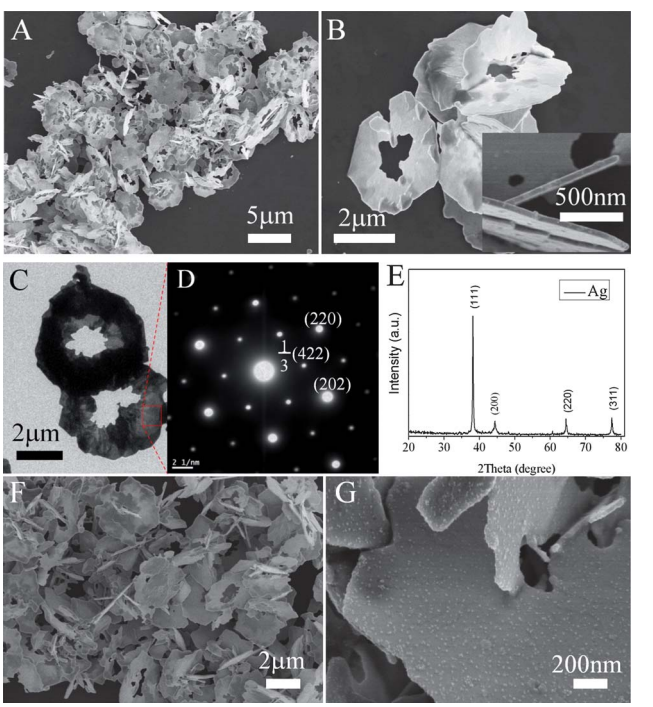

Fig. 2 SEM (A and B) and TEM (C and D) images and XRD pattern (E) of pristine Ag HMDs. (F) and (G) are SEM images of ZnO seed-coated Ag HMDs.

assistance of PVP for subsequent ZnO NR growth. As shown in Fig. 2F, the Ag HMDs are still in good dispersity after ZnO seed loading. From Fig. 2G at a high magnification, it can be seen that the Ag HMDs were uniformly covered by a layer of well dispersed ZnO seeds with the size estimated to be several nanometers, indicating the successful coating of ZnO seeds on the surfaces of Ag HMDs. This is important for subsequent ZnO NR growth and the preparation of the hierarchical ZnO/Ag heterostructure shown in Fig. 1.

It is found that the diameter and length of ZnO NRs are significantly influenced by their growth time. As shown in Fig. 3A, after 2 h of the reaction, the Ag/ZnO heterostructures consisting of short ZnO NRs arrayed on Ag HMDs were formed. A high-magnification image in Fig. 3B reveals that the ZnO NRs were about 30 nm in diameter and 600–800 nm in length, which is much thinner and shorter than the typical products shown in Fig. 1. The Ag HMDs of the heterostructures in this case can be observed, as marked out in Fig. 3B, due to the thinner diameter of the ZnO NRs that lead to a relatively loose covering. When the growth time was increased to as long as 24 h, densely packed Ag/ZnO heterostructures with a bush-like morphology were obtained (Fig. 3C and D). The ZnO NRs became much thicker and longer after growth, *i.e.* with an average diameter of 150 nm and length of 1.8 μm, respectively. The results indicate that the diameter and length, as well as the coverage of ZnO NRs increased monotonically with increasing their growth time. In addition, most ZnO NRs obtained at 24 h show sharp tips, which is distinctly different from those obtained with a short growth time and may find specific applications, such as field emitters.

On the other hand, the nutrient concentration of zinc nitrate also plays a prominent role in determining the structures of ZnO NRs and heterostructures of Ag HMDs/ZnO NRs. At a lower concentration of 2 mM, shorter ZnO NRs with concave tips (indicated by the red arrows) were formed on Ag HMDs (Fig. $4A_1$ and A_2). The diameter and length of these shorter ZnO NRs were not uniform, ranging from 50–200 nm and 100–200 nm (Fig. $4A_2$), respectively. When the concentration of zinc nitrate was increased to 5 mM, the ZnO NRs became obviously longer and thinner, for example, 20–150 nm in diameter and 150–300 nm in length (Fig. $4B_1$ and B_2). Interestingly, many ZnO NRs possessed a tubular tip, as denoted by the red arrows in Fig. $4B_2$. When the nutrient concentration was further increased to 8 mM and 10 mM, much longer ZnO NRs (400–800 nm in length) with solid tips and dense and ordered covering were evident (Fig. $4C_1$, C_2, D_1 and D_2). This seems to suggest that lower nutrition concentrations (*ca.* 2–5 mM) are preferable for the formation of concave or tubular, shorter ZnO NRs on Ag HMDs, while higher concentrations (*ca.* 8–10 mM) favor the generation of solid longer ZnO NRs. It was reported by Zeng and Liu that such unusual ZnO NRs with concave or tubular tips were preferably formed under kinetically controlled growth processes at high reactant concentrations, because precursor species preferentially deposited on the rims of NRs, due to a shorter distance to the rims than to the central regions of the NRs.[35] Nevertheless, in this work, the ZnO NRs with concave or tubular tips obtained at low reactant concentrations gave a different result. This is probably ascribed to a different hollowing mechanism of ZnO NRs described below. In our work, abundant ZnO seeds were precoated onto Ag HMDs and served as nucleation sites for ZnO NR growth. Relatively, ZnO precursors at low concentrations are insufficient to feed ZnO crystallites nucleated at these sites for their consecutively growing into longer ZnO NRs, thereby leading to the shorter ZnO NR

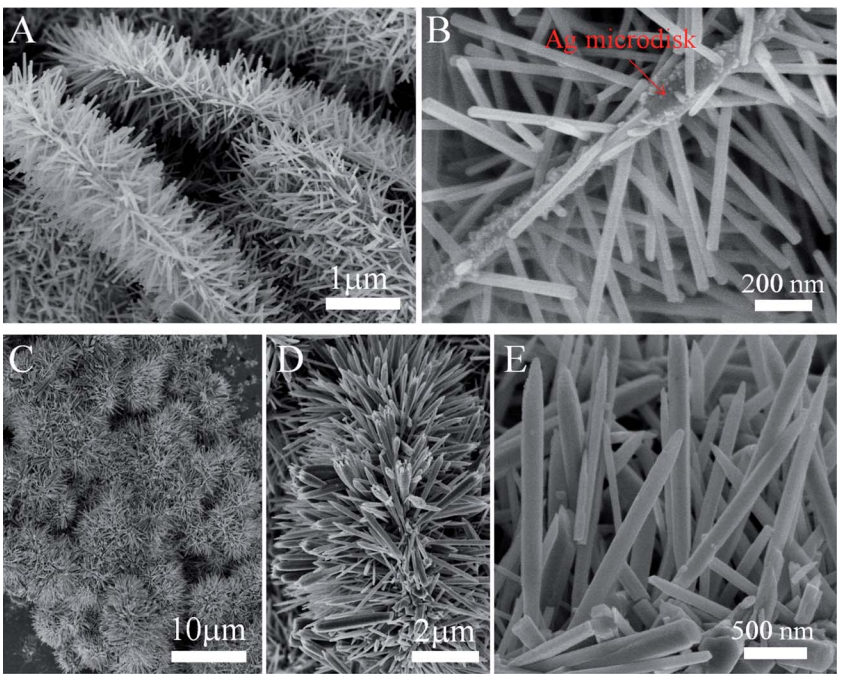

Fig. 3 SEM images of Ag HMD/ZnO NR heterostructures formed under the typical conductions except at different growth times. (A and B): 2 h; (C–E): 24 h.

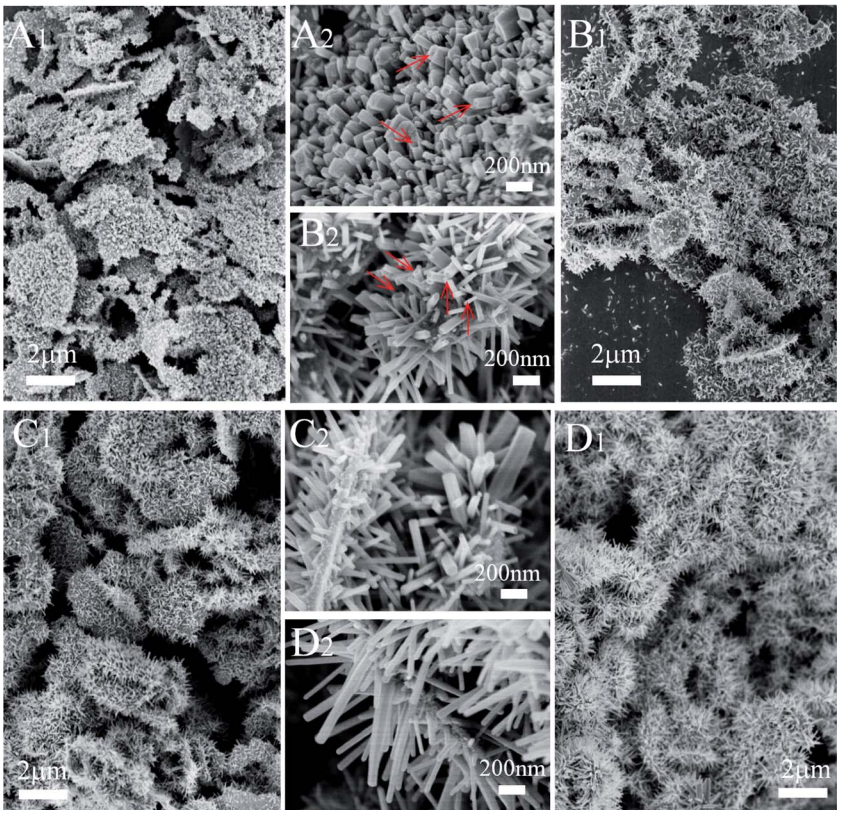

Fig. 4 SEM images of Ag HMD/ZnO NR heterostructures formed after 5 h with different nutrition concentrations of zinc nitrate for ZnO NR growth. (A_1 and A_2): 2 mM; (B_1 and B_2): 5 mM; (C_1 and C_2): 8 mM; (D_1 and D_2): 10 mM.

formation, as also can be referred to in Fig. 4A_1, A_2, B_1 and B_2. Compared with longer NRs, these shorter ZnO NRs are much less stable, especially their exposed active polar (0002) planes. Driven by energy minimization, these active atoms in (0002) planes were "dissolved" and "redeposited" gradually to the relatively stable ($10\bar{1}0$) planes of the side surface, *i.e.*, the rim area of the ZnO NRs, resulting in the formation of the concave or tubular ZnO NRs.

The typical Ag HMD/ZnO NR heterostructure in Fig. 1 prepared at 10 mM concentration after 8 h growth was investigated for its photocatalytic property through RhB degradation under irradiation of a Hg lamp (300 W). The heterocatalyst was deposited on an (2 cm × 2 cm) ITO substrate and the corresponding mass on the ITO substrate was measured to be a very small amount of 2.8 mg. Fig. 5A presents the UV-vis absorption spectra of RhB solution recorded at different degradation times with the typical Ag HMDs/ZnO NRs as the catalyst. As can be seen, the maximum absorbance (554 nm) of RhB in the solution decreases gradually with exposure time and finally goes to the baseline at ~180 min, which indicates the RhB in the solution can be degraded completely by the Ag/ZnO heterocatalyst within 3 h. Since the Ag/ZnO heterostructures consisted of Ag HMDs and ZnO NRs, other different samples such as bare Ag HMDs, dispersed ZnO NRs and ordered ZnO NR arrays on ITO substrates have been fabricated by similar methods (S2, S3 and Fig. S1†) and photocatalysis was conducted for direct comparison. It is noted that all the samples were normalized to the same area (2 cm × 2 cm) as the ITO substrate. The photocatalytic properties of these nanostructures are demonstrated in Fig. 5B. In principle, the degradation process approximately complies with the pseudo-first-order kinetics

$$\ln\left(\frac{C}{C_0}\right) = -kt \quad (1)$$

where C_0, C and k are the initial concentration of RhB, the real concentrations of RhB corresponding to the exposure time t and the degradation constant, respectively. k values of fitted degradation lines for different nanostructures of Ag HMDs/ZnO NRs, dispersed ZnO NRs, ZnO NR arrays, Ag HMDs and blank (no catalyst added) were calculated to be 0.0208, 0.0144, 0.0137, 0.0030, 0.0026 min^{-1}, respectively. The results indicate that the photocatalytic efficiency for the Ag HMD/ZnO NR heterocatalyst was about 1.5 times that relative to the bare ZnO catalysts (dispersed ZnO NRs and ZnO NR arrays) (Fig. S1†). Since Ag HMDs are nearly inert in the process of RhB photodegradation, the excellent photocatalytic activity of the Ag HMDs/ZnO NRs is attributed to the Ag/ZnO heterostructure that favors effective generation, separation and transfer of photoinduced charges at Ag–ZnO interfaces and thus reduces recombination of electrons and holes (Fig. 5C).[24,30,36] Fig. S2† presents the photoluminescence spectra of the bare ZnO NR arrays and the typical heterostructure of Ag HMDs/ZnO NR arrays, where a strong band emission (~400 nm) and a weak green emission (~570 nm) are observed for both samples. The emission peaks

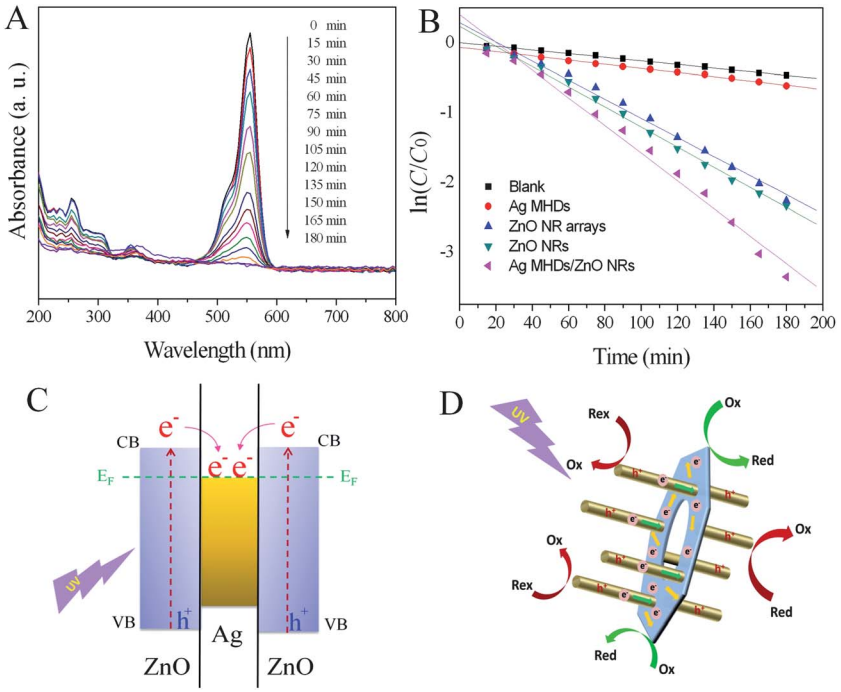

Fig. 5 (A) Examples of RhB degradation data with time under UV-light irradiation in the presence of catalyst of typical Ag HMD/ZnO NR heterostructure. (B) The photocatalytic properties of the typical hierarchical Ag HMD/ZnO NR heterostructure, as well as the blank (no catalyst added), the bare Ag HMDs, ZnO NRs and ZnO NS arrays which were cast or grown on the ITO substrates (2 cm × 2 cm). (C) Schematic illustrations for the photo-induced charge separation of Ag HMD/ZnO NRs heterostructures. (D) The speculated photocatalytic mechanism of the Ag HMD/ZnO NR heterostructures.

around two positions are caused by the recombination of the electrons in the CB (conduction band) and defect levels of ZnO with the holes in the VB (valence band),[37] respectively. Moreover, compared with the bare ZnO NRs, the intensities of the band and green emissions of the Ag/ZnO heterostructure are lower, which indicates the relative population of electrons in CB and defects are significantly decreased.[38] This result implies that both CB and defect electrons can readily transfer to Ag HMDs *via* Ag–ZnO interfaces under excitation. Therefore, it can be envisaged that under UV irradiation, photoelectrons generated from the double-sided ZnO NR arrays will inject quickly into Ag HMDs, while photoholes are left in the ZnO NRs (Fig. 5C); in this process, ZnO NR arrays and Ag HMDs work as both 1D/2D spatial pathways for fast electron transport and spatial active sites for efficient catalytic oxidative and reductive reactions (Fig. 5D). The rapid proceeding of the oxidative and reductive half reactions leads to the high efficiency of photocatalysis. We emphasize here that double-sided ZnO NR arrays with an opened structure can offer more accessible active sites, which is beneficial for the full adsorption/degradation of RhB molecules; meanwhile, the holes in the Ag HMDs can facilitate molecular diffusion, which is helpful for enhanced catalytic kinetics. In addition, compared with our previously reported Ag NW/ZnO NR heterostructures where ZnO NR arrays were grown on 1D Ag core NWs,[30] the typical Ag HMD/ZnO NR catalyst in this work exhibits a higher photocatalytic activity with the efficiency being almost doubled. We think this remarkable improvement is likely to be resulted from the unique 2D structure of Ag HMDs which promotes a faster and more efficient electron transport and export, and significantly enhances the chance for electron acceptors to grasp electrons, as shown in Fig. 5D. In brief, firstly, a Ag HMD connects more ZnO NRs than a Ag NW, offering more integrated Ag–ZnO heterojunctions for better photoinduced hole–electron separation. Secondly, Ag microdisks can be equivalent to two-dimensional planes consisting of a large number of interwoven one-dimensional Ag NWs and serve as spatially extended electron active centers for electron acceptors. As 2D structured electron active centers, Ag HMDs have more chances to be reached by some molecules/ions of the electron acceptors, such as O_2^- ions and radicals. It can be imagined that once these electron acceptors diffuse to these 2D active centers of Ag HMDs, electrons can be transferred directly from the disk and the reductive half reactions can be performed, which actually improves the reaction chances and thus prompts the catalysis to proceed.

4 Conclusions

In summary, the novel hierarchical Ag/ZnO heterostructures with double-sided ZnO NR arrays grown on Ag HMDs have been fabricated *via* a ZnO-seeded heteroepitaxial growth of ZnO NRs on Ag HMDs. The structural parameters such as diameter, length and shape of ZnO NRs in heterostructures can be tuned by simply adjusting the reactant concentration and the growth time. Moreover, the typical heterostructure of Ag HMDs/ZnO NRs showed excellent photocatalytic activity in the photocatalytic measurements of RhB degradation, compared with the other catalysts made of bare ZnO NRs or the heterocatalyst of

the Ag NWs/ZnO NRs. The remarkable improvement in photocatalytic efficiency is ascribed to the synergistic contribution of the unique structure of the Ag HMDs/ZnO NRs, such as high SSA supplying abundant active sites for effective catalysis, 1D/2D ZnO NR/Ag HMD structures with integrated contact for effective charge separation and high rate 1D/2D electron transport, and special spatial configuration consisting of double sided NR arrays and holed microdisks with an opened and accessible architecture for effective diffusion and full adsorption of small molecules. With these structural advantages, the novel Ag/ZnO heterostructures when made with some suitable modifications are also promising in many related areas such as energy conversion and storage (solar cells, lithium batteries, water splitting), electro-chemiluminescence sensors and so on.

Acknowledgements

This work was financially supported by the National Natural Science Foundation (21001082, 21273161 and 21101117), Shanghai Innovation program (13ZZ026), Scientific Research Foundation for the Returned Overseas Chinese Scholars of SEM, Shanghai Pujiang Program (10PJ1410400), Research Fund for the Doctoral Program of Higher Education of China (20090072120013), Visiting scholar fund of the Key Laboratory for Ultrafine Materials of Ministry of Education, East China University of Science and Technology, and the Fundamental Research Funds for the Central Universities.

References

1 T. Mokari, E. Rothenberg, I. Popov, R. Costi and U. Banin, *Science*, 2004, **304**, 1787.
2 T. Mokari, C. G. Sztrum, A. Salant, E. Rabani and U. Banin, *Nat. Mater.*, 2005, **4**, 855.
3 S. E. Habas, P. D. Yang and T. J. Mokari, *J. Am. Chem. Soc.*, 2008, **130**, 3294.
4 F. R. Fan, Y. Ding, D. Y. Liu, Z. Q. Tian and Z. L. Wang, *J. Am. Chem. Soc.*, 2009, **131**, 12036.
5 K. Sun, Y. Jing, N. Park, C. H. Li, Y. S. Bando and D. L. Wang, *J. Am. Chem. Soc.*, 2010, **132**, 15465.
6 L. Wu, B. G. Quan, Y. L. Liu, R. Song and Z. Y. Tang, *ACS Nano*, 2011, **5**, 2224.
7 J. Yang and J. Y. Ying, *Angew. Chem., Int. Ed.*, 2011, **50**, 4637.
8 L. Shi, Y. M. Xu, S. K. Hark, Y. Liu, S. Wang, L. M. Peng, K. W. Wong and Q. Li, *Nano Lett.*, 2007, **7**, 3559.
9 Y. Y. Ma, W. Y. Li, E. C. Cho, Z. Y. Li, T. Yu, J. Zeng, Z. X. Xie and Y. N. Xia, *ACS Nano*, 2010, **4**, 6725.
10 M. Mckiernan, J. Zeng, S. Ferdous, S. Verhaverbeke, K. S. Leschkies, R. Gouk, C. Lazik, M. Jin, A. L. Briseno and Y. N. Xia, *Small*, 2010, **6**, 1927.
11 C. Pacholski, A. Kornowski and H. Weller, *Angew. Chem., Int. Ed.*, 2004, **43**, 4774.
12 J. S. Lee, E. V. Shevchenko and D. V. Talapin, *J. Am. Chem. Soc.*, 2008, **130**, 9673.
13 Y. G. Sun and Y. N. Xia, *Adv. Mater.*, 2002, **14**, 833.
14 A. Tao, F. Kim, C. Hess, J. Goldberger, R. R. He, Y. G. Sun, Y. N. Xia and P. D. Yang, *Nano Lett.*, 2003, **3**, 1229.
15 H. Y. Shi, B. Hu, X. C. Yu, R. L. Zhao, X. F. Ren, S. L. Liu, J. W. Liu, M. Feng, A. W. Xu and S. H. Yu, *Adv. Funct. Mater.*, 2010, **20**, 958.
16 Y. G. Sun, *Nanoscale*, 2010, **2**, 1626.
17 A. I. Hochbaum and P. D. Yang, *Chem. Rev.*, 2010, **110**, 527.
18 M. H. Huang, S. Mao, H. Feick, H. Q. Yan, Y. Y. Wu, H. Kind, E. Weber, R. Russo and P. D. Yang, *Science*, 2001, **292**, 1897.
19 Z. W. Pan, Z. R. Dai and Z. L. Wang, *Science*, 2001, **291**, 1947.
20 Z. L. Wang and J. H. Song, *Science*, 2006, **312**, 242.
21 S. H. Ko, D. Lee, H. W. Kang, K. H. Nam, J. Y. Yeo, S. J. Hong, C. P. Grigoropoulos and H. J. Sung, *Nano Lett.*, 2011, **11**, 666.
22 C. K. Xu, J. M. Wu, U. V. Desai and D. Gao, *J. Am. Chem. Soc.*, 2011, **133**, 8122.
23 C. L. Ren, B. F. Yang, M. Wu, J. Xu, Z. P. Fu, Y. Lv, T. Guo, Y. X. Zhao and C. Q. Zhu, *J. Hazard. Mater.*, 2010, **182**, 123.
24 C. D. Gu, C. Cheng, H. Y. Huang, T. L. Wong, N. Wang and T. Y. Zhang, *Cryst. Growth Des.*, 2009, **9**, 3278.
25 M. J. Height, S. E. Pratsinis, O. Mekasuwandumrong and P. Praserthdam, *Appl. Catal., B*, 2006, **63**, 305.
26 C. Karunakaran, V. Rajeswari and P. Gomathisankar, *Solid State Sci.*, 2011, **13**, 923.
27 L. B. Hu, H. S. Kim, J. Y. Lee, P. Peumans and Y. Cui, *ACS Nano*, 2010, **4**, 2955.
28 C. Yang, H. W. Gu, W. Lin, M. M. Yuen, C. P. Wong, M. Y. Xiong and B. Gao, *Adv. Mater.*, 2011, **23**, 3052.
29 J. Yin, Y. S. Zang, C. Yue, Z. M. Wu, S. T. Wu, J. Li and Z. H. Wu, *J. Mater. Chem.*, 2012, **22**, 7902.
30 S. W. Wang, Y. Yu, Y. H. Zuo, C. Z. Li, J. H. Yang and C. H. Lu, *Nanoscale*, 2012, **4**, 5895.
31 J. H. Yang, L. M. Qi, D. B. Zhang, J. M. Ma and H. M. Cheng, *Cryst. Growth Des.*, 2004, **4**, 1371.
32 J. H. Yang, G. M. Liu, J. Lu, Y. F. Qiu and S. H. Yang, *Appl. Phys. Lett.*, 2007, **90**, 103109.
33 J. H. Yang, Y. F. Qiu and S. H. Yang, *Cryst. Growth Des.*, 2007, **7**, 2562.
34 F. Li, Y. Ding, P. X. Gao, X. Q. Xin and Z. L. Wang, *Angew. Chem., Int. Ed.*, 2004, **43**, 5238.
35 B. Liu and H. C. Zeng, *Nano Res.*, 2009, **2**, 201.
36 Y. H. Zheng, L. R. Zheng, Y. Y. Zhan, X. Y. Lin, Q. Zheng and K. M. Wei, *Inorg. Chem.*, 2007, **46**, 6980.
37 J. Im, J. Singh, J. W. Soares, D. M. Steeves and J. E. Whitten, *J. Phys. Chem. C*, 2011, **115**, 10518.
38 S. T. Kochuveedu, J. H. Oh, Y. R. Do and D. H. Kim, *Chem.–Eur. J.*, 2012, **18**, 7467.

